Monthly Notices of the ROYAL ASTRONOMICAL SOCIETY

MNRAS **510,** 3011–3018 (2022) https://doi.org/10.1093/mnras/stab3598
Advance Access publication 2021 December 13

Destruction of AlF: a quantum study of its ground-state photodissociation

Zhi Qin [1,2,3] Tianrui Bai[1,3] and Linhua Liu [1,3,4]★

[1]*Optics and Thermal Radiation Research Center, Institute of Frontier and Interdisciplinary Science, Shandong University, Qingdao, Shandong 266237, China*
[2]*School of Information Science and Engineering, Shandong University, Qingdao, Shandong 266237, China*
[3]*School of Energy and Power Engineering, Shandong University, Jinan, Shandong 250061, China*
[4]*School of Energy Science and Engineering, Harbin Institute of Technology, Harbin, Heilongjiang 150001, China*

Accepted 2021 December 7. Received 2021 December 6; in original form 2021 October 23

ABSTRACT

Photodissociation by ultraviolet photons is the key destruction pathway for aluminium monofluoride (AlF) in the envelope of the carbon star IRC +10216 from the stellar photosphere up to the outer layers. However, there is no available photodissociation data for AlF, which hampers the prediction of the abundances of Al-bearing molecules in astrochemical models. Here, we present an *ab initio* study of AlF photodissociation. Potential energy curves of seven singlet states for AlF were computed by the internally contracted multireference single and double configuration-interaction method and aug-cc-pCV5Z-DK basis set, along with the transition dipole moments from excited singlet states to the ground state. State-resolved cross sections for the direct photodissociation from 36 349 ground rovibrational levels ($\upsilon'' \leq 120$, $J'' \leq 360$) to six singlet excited states were calculated by the quantum mechanical method. We found that the $2^1\Pi \leftarrow X\ ^1\Sigma^+$, $3^1\Pi \leftarrow X\ ^1\Sigma^+$, and $4^1\Pi \leftarrow X\ ^1\Sigma^+$ transitions have extremely strong absorption for lower wavelengths, especially between the Lyman and Lyman α ones. Photodissociation cross sections in local thermal equilibrium were estimated for gas temperatures from 500 to 20 000 K. Finally, the cross sections were utilized to calculate the photodissociation rates in the interstellar and blackbody radiation fields. The obtained photodissociation cross sections and rates can be used to determine the abundance of AlF in astrochemical models.

Key words: astrochemistry – molecular data – molecular processes – ISM: molecules.

1 INTRODUCTION

As the 12th most abundant element in space, aluminium (Al) has been observed in dense warm molecular clouds (Turner 1991) and circumstellar environments (Mauron & Huggins 2010). The Al element is depleted substantially into grains in dense molecular clouds, while this element exhibits significant gas-phase chemistry in carbon-rich circumstellar environments. In the circumstellar envelope of the asymptotic giant branch (AGB) carbon star IRC +10216, the millimetre spectra of Al-bearing molecules, such as AlCl, AlF, and AlNC, have been observed (Cernicharo & Guélin 1987; Ziurys, Apponi & Phillips 1994; Ziurys et al. 2001; Mauron & Huggins 2010; Agúndez et al. 2012). Moreover, aluminium monofluoride (AlF) has been also observed in the AGB wind of CRL 2688 (Highberger et al. 2001) and the sunspot umbrae (Bagare, Kumar & Rajamanickam 2006). Recently, millimetre-wave rotational lines of the isotopologue of AlF have been observed towards CK Vul, a remnant of a stellar merger (Kamiński et al. 2018). Observations show that AlF is found in distant shells in the envelope of IRC + 10216 (Mauron & Huggins 2010; Agúndez et al. 2012; Andreazza & de Almeida 2014), which is a photodissociation region and may lead to photochemistry reactions of AlF. The photodissociation of AlF may likely occur by absorbing a photon

$$\mathrm{AlF} + h\upsilon \rightarrow \mathrm{Al} + \mathrm{F}. \quad (1)$$

Photodissociation processes are found to be very important in modelling the evolution of chemical composition in any region exposed to intense ultraviolet (UV) radiation, such as diffuse and translucent interstellar clouds, high-velocity shocks, the surface layers of protoplanetary disks, and so on (Schlemmer et al. 2014; Heays, Bosman & van Dishoeck 2017). After absorbing a single photon, molecules like AlF will undergo direct dissociation processes, which can impact the abundance of the related compositions (Heays et al. 2017; Gao 2020; Valiev et al. 2020). The produced species resulted from these processes are usually chemically reactive and then involved in the formation of other Al-bearing species (Mauron & Huggins 2010; Agúndez et al. 2012). Due to no available photodissociation rates for AlF, Agúndez et al. (2012) adopted the educated guess value to predict its abundance in the circumstellar envelope of the carbon star IRC + 10216. In the recent collection of photodissociation and photoionization cross sections of atoms and molecules of astrophysical interest by Heays et al. (2017), AlF is not included. Hence, the quantitative evaluation of the photodissociation processes for AlF is required to securely estimate its abundance and provide an in-depth understanding of gas-phase chemistry in the carbon star envelope IRC + 10216 (Mauron & Huggins 2010; Agúndez et al. 2012).

Wavelength-dependent cross sections and rate coefficients are fundamental quantities for governing photodissociation processes and are required to derive the abundance of related species. In previous studies of AlF, Gotoum et al. (2011, 2012) computed the rotational excitation cross sections and rate coefficients of AlF collisions with He up to the temperature of 300 K and with

★ E-mail: liulinhua@sdu.edu.cn

para-H_2 up to the temperature of 70 K. Besides, the rate coefficients for the formation of AlF by radiative association, an inverse process of equation (1), were presented by Andreazza & Almeida (2014). However, to our knowledge, there seems to be no information about the photodissociation cross sections and rates of AlF, which limits the prediction of the abundance for AlF in carbon-rich stellar environments.

In this work, wavelength-dependent cross sections of the AlF molecule are presented for several electronic transitions from a wide range of ground rovibrational levels. Dipole-allowed transitions from the $2^1\Sigma^+$, $3^1\Sigma^+$, $A^1\Pi$, $2^1\Pi$, $3^1\Pi$, and $4^1\Pi$ states to the ground $X^1\Sigma^+$ state are investigated here. The potential energy curves (PECs) and transition dipole moments (TDMs) for these electronic states are obtained by the state-of-the-art *ab initio* methods. The cross sections are then obtained by utilizing quantum mechanical techniques based on the PECs and TDMs. Applications of the cross sections to environments in local thermal equilibrium (LTE) conditions are also given. Finally, cross sections are used to compute the photodissociation rates of AlF in the standard interstellar radiation field (ISRF) and the blackbody radiation field.

2 THEORY AND METHODS

2.1 Ab initio calculations

Using the high-level *ab initio* calculations implemented in the MOLPRO 2015 software package (Werner et al. 2015, 2020), the electronic structures of AlF have been determined. Thus, the PECs and TDMs for seven singlet states have been investigated by employing the complete active space self-consistent field (CASSCF) method (Knowles & Werner 1985; Werner & Knowles 1985) followed by the internally contracted multireference single and double configuration-interaction (icMRCI) method with Davidson correction (+Q). The Al atom, consisting of 13 electrons, and the F atom, consisting of 9 electrons, were treated in the following way: Using the augmented correlation consistent polarized core valence quintuplet aug-cc-pCV5Z-DK Gaussian basis set, 10 electrons were closed within the core of Al and 2 electrons were closed within the core of F. The remaining eight electrons were considered as active electrons within the considered molecular orbitals. The scalar relativistic effect is taken into account by the third-order Douglas–Kroll Hamiltonian (Reiher & Wolf 2004a,b). The symmetric point group of AlF is $C_{\infty v}$. Due to the limitation of the MOLPRO software package, the C_{2v} point group, an Abelian subgroup of $C_{\infty v}$, is selected for the electronic structure calculation of AlF. Thus, eight active electrons were put into the active space distributed into the irreducible representation a_1, b_1, b_2, and a_2 as (6, 2, 2, 0). In the calculations of PECs and TDMs, 81 points for $^1\Sigma^+$ states with the internuclear distance in the range of 1.05–8 Å were considered. The step length is 0.05 Å for $R = 1.05$–1.4 Å, 0.02 Å for $R = 1.4$–1.8 Å, 0.05 Å for $R = 1.8$–2.6 Å, 0.1 Å for $R = 2.6$–6.0 Å, and 0.5 Å for $R = 6$–8 Å. For $^1\Pi$ states, the PECs tend to their dissociation limits at $R > 4$ Å, and the step length of 0.5 Å is selected to reduce computing resources.

2.2 Photodissociation theory

Based on the Born–Oppenheimer approximation, the Schrödinger equation is separable into the fixed nuclei electronic motion equation and the nuclear motion equation. The electronic motion equation is solved to varying degrees of approximation by using standard *ab initio* techniques, some of which used in this work are mentioned in Section 2.1. The obtained PEC provides the potential energy term in the nuclear motion equation to determine the rovibrational wavefunction $\chi_{\upsilon'' J''}(R)$ for a bound electronic state and the continuum wavefunction $\chi_{k' J'}(R)$ for an electronic state with no potential well. The state-resolved photodissociation cross section for an electric dipole transition from a bound state i with rovibrational levels $\upsilon'' J''$ to a free state f can be written as

$$\sigma^{fi}_{\upsilon'' J''}\left(E_{\rm ph}\right) = \frac{4\pi^2 e^2}{3\hbar c} E_{\rm ph} g \sum_{J'} \left(\frac{1}{2J''+1} S_{J'}\left(J''\right) \left|\left\langle \chi_{k' J'}(R) \left| D^{fi}(R) \right| \chi_{\upsilon'' J''}(R) \right\rangle\right|^2\right), \quad (2)$$

in which e is the electron charge, $\hbar$ is the reduced Planck constant, c is the speed of light in vacuum, $E_{\rm ph}$ is the photon energy, g is the degeneracy factor, $S_{J'}(J'')$ is the Hönl–London factors (Hansson & Watson 2005; Watson 2008), and $D^{\rm fi}(R)$ is the TDM. The bound rovibrational wavefunctions are normalized to unity and vanish at zero and infinity. The continuum wavefunctions behave asymptotically as

$$\chi_{k' J'}\left(R \text{ large}\right) \approx \sqrt{\frac{2\mu}{\hbar^2 \pi k'}} \sin\left[k' R - \frac{1}{2} J' \pi + \delta_J\left(E'\right)\right], \quad (3)$$

where $\delta_J(E')$ is the phase shift at the continuum energy E', $k' = |\boldsymbol{k}'|$is the magnitude of the wavevector $\boldsymbol{k}'$, given by

$$k' = \sqrt{2\mu E'}. \quad (4)$$

If the environments including AlF are in LTE, a Boltzmann population distribution is assumed for the rovibrational levels in the electronic ground state. It is important to consider the LTE cross section

$$\sigma\left(\lambda, T\right) = \frac{\sum_{\upsilon'' J''} \left(2J''+1\right) \exp\left(-\left|E_{\upsilon'' J''} - E_{00}\right| / k_{\rm b} T\right) \sigma^{fi}_{\upsilon'' J''}}{\sum_{\upsilon'' J''} \left(2J''+1\right) \exp\left(-\left|E_{\upsilon'' J''} - E_{00}\right| / k_{\rm b} T\right)}, \quad (5)$$

where $E_{\upsilon'' J''}$ is the magnitude of the bonding energy of the rovibrational level $\upsilon'' J''$, $k_{\rm b}$ is the Boltzmann constant, and the denominator denotes the rovibrational partition function.

The computed cross sections can be used to evaluate the photodissociation rate of a molecule exposed to a UV radiation field

$$k = \int \sigma\left(\lambda\right) I\left(\lambda\right) {\rm d}\lambda, \quad (6)$$

where $\sigma(\lambda)$ is the appropriate photodissociation cross sections and $I(\lambda)$ is the photon-based radiation intensity, whose expressions are different depending on different radiation fields. For the blackbody radiation field, the intensity is given by the Planck law (Heays et al. 2017; Pattillo et al. 2018). For the ISRF, the average radiation intensity is given by Draine (1978) and van Dishoeck & Black (1982).

Above is a brief overview of the photodissociation theory. Detailed descriptions can be found in previous publications (Van Dishoeck & Black 1988; Kirby & Van Dishoeck 1989; Stancil et al. 1997; Weck, Stancil & Kirby 2003; Miyake, Gay & Stancil 2011; Gay et al. 2012; El-Qadi & Stancil 2013; Babb 2015; McMillan et al. 2016; Heays et al. 2017; Pattillo et al. 2018; Bai, Qin & Liu 2021; Qin, Bai & Liu 2021a).

3 RESULTS AND DISCUSSION

3.1 PECs and TDMs

Based on the icMRCI/aug-cc-pCV5Z-DK method, seven singlet electronic states have been investigated and presented in Fig. 1, where the potential energies are plotted as a function of the internuclear distance R. The $X^1\Sigma^+$, $2^1\Sigma^+$, $A^1\Pi$, and $2^1\Pi$ states correlate

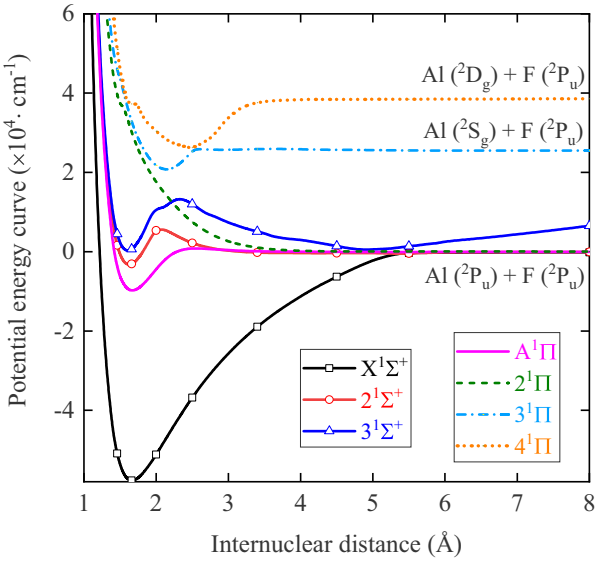

Figure 1. The PECs of the $X^1\Sigma^+$, $A^1\Pi$, $2^1\Sigma^+$, $3^1\Sigma^+$, $2^1\Pi$, $3^1\Pi$, and $4^1\Pi$ states for AlF obtained by the icMRCI + Q calculation in the active space [(10, 3, 3, 0)–(4, 1, 1, 0)] with the aug-cc-pCV5Z-DK basis set. The symbols on the PECs of the $^1\Sigma^+$ states are data points displayed by skipping 10 points. All the data points are detailed in the text and provided in the supplemental material.

with the first molecular dissociation asymptote. The $3^1\Pi$ and $4^1\Pi$ states dissociate to the third and fourth dissociation asymptotes, respectively. These three asymptotes result from the combination of the atomic states [Al ($3s^2 3p\ ^2P$) + F ($2s^2 2p^5\ ^2P$), Al ($3s^2 4s\ ^2S$) + F ($2s^2 2p^5\ ^2P$), and Al ($3s^2 3d\ ^2D$) + F ($2s^2 2p^5\ ^2P$)]. It is noted that the $3^1\Sigma^+$ state correlates to the second dissociation limit, which corresponds to a polarized state for which AlF dissociates into its ionic fragments [Al^+ ($3s^{2\,1}S$) + F^- ($2s^2 2p^{6\,1}S$)]. The dissociation relationships of these seven states are presented in Table 1. To check the precision of our calculations, a comparison between our calculated asymptotic energies and those available in the NIST Atomic Spectra Database (Kramida et al. 2020) is performed in Table 1. An overall good agreement is observed in which the percentage relative difference is about 0.3 per cent for the third dissociation limit. For the $3^1\Sigma^+$ state, it does not seem to dissociate completely at the internuclear distance of 8 Å. Calculations of the PECs at larger internuclear distances failed due to the convergence problem. The experimental asymptotic energy for the second dissociation limit is 20845.962 cm^{-1}, which is obtained from Martin & Zalubas (1979) and Yang et al. (2005) and is used in the calculations of cross sections below.

As shown in Fig. 1, the avoided crossing occurs between the $2^1\Pi$ and $3^1\Pi$ states, also between the $3^1\Pi$ and $4^1\Pi$ states. This behaviour can be illustrated as follows: Two electronic states of the same spin quantum number but of different symmetry can cross each other because their wavefunctions are orthogonal; the eigenvalues of solving the Schrödinger equation for these two states can be equal. Similarly, two states with different spin quantum numbers but of the same symmetry can also exhibit an allowed crossing. However, two states having the same spin quantum number and symmetry show avoided crossing because their eigenvalues cannot be equal.

The spectroscopic constants for the $X^1\Sigma^+$, $A^1\Pi$, $2^1\Sigma^+$, and $3^1\Sigma^+$ states have been calculated by fitting the energy data and are reported in Table 2, together with available experimental and theoretical results for comparison. For the ground state, the calculated equilibrium internuclear distance R_e is 1.6639 Å, which is somewhat larger than the experimental value of 1.654 Å (Zhang et al. 1995) and agrees reasonably with available theoretical ones with relative differences of 0.62 per cent (Yousefi & Bernath 2018), 1.56 per cent (Wells & Lane 2011), and 0.91 per cent (Langhoff, Bauschlicher & Taylor 1988). The calculated harmonic frequency ω_e of 801.64 cm^{-1} is in good agreement with the experimental one of 802.4391 cm^{-1} (Barrow, Kopp & Malmberg 1974) and the recent theoretical value of 806.35 cm^{-1}. Moreover, there is good conformity in the values of the rotational constant B_e between our result and those in the experiment and calculations. The relative deviations are 1.3 per cent (Barrow et al. 1974), 1.4 per cent (Yousefi & Bernath 2018), and 3.2 per cent (Wells & Lane 2011). For the $A^1\Pi$ state, a good agreement with the experimental and theoretical values (Barrow et al. 1974; Wells & Lane 2011) is also observed for the spectroscopic constants. For the $2^1\Sigma^+$ and $3^1\Sigma^+$ states, our calculations improve the spectroscopic constants a lot relative to those calculated by Wells & Lane (2011), by comparing with the experimental ones (Barrow et al. 1974). Such improvement can be attributed to the high-level icMRCI/aug-cc-pCV5Z-DK calculation.

The TDMs of six singlet transitions from the $2^1\Sigma^+$, $3^1\Sigma^+$, $A^1\Pi$, $2^1\Pi$, $3^1\Pi$, and $4^1\Pi$ states to the ground state are shown in Fig. 2 as a function of the internuclear distance. A comparison of the TDM for the $A^1\Pi$–$X^1\Sigma^+$ transition with that computed by Langhoff et al. (1988) has been made and displayed in Fig. 3. For the internuclear distances smaller than 2 Å, our TDMs are in good agreement with

Table 1. Dissociation relationships of the $X^1\Sigma^+$, $A^1\Pi$, $2^1\Sigma^+$, $3^1\Sigma^+$, $2^1\Pi$, $3^1\Pi$, and $4^1\Pi$ states for AlF.

Molecular state	Dissociation limit				
	Atomic state	Energy (cm^{-1})[a]	Energy (cm^{-1})[b]	C_5[c]	C_6[c]
$X^1\Sigma^+$	Al ($3s^2 3p\ ^2P$) + F ($2s^2 2p^5\ ^2P$)	0.00	0.00	19.6	75.23
$A^1\Pi$	Al ($3s^2 3p\ ^2P$) + F ($2s^2 2p^5\ ^2P$)	0.00	0.00	8.07	75.23
$2^1\Sigma^+$	Al ($3s^2 3p\ ^2P$) + F ($2s^2 2p^5\ ^2P$)	0.00	0.00	7.33	75.23
$2^1\Pi$	Al ($3s^2 3p\ ^2P$) + F ($2s^2 2p^5\ ^2P$)	0.00	0.00	7.17	75.23
$3^1\Sigma^+$	Al^+ ($3s^{2\,1}S$) + F^- ($2s^2 2p^{6\,1}S$)	20845.962[d]	–	0.00	−153.35
$3^1\Pi$	Al ($3s^2 4s\ ^2S$) + F ($2s^2 2p^5\ ^2P$)	25347.756	25422.60	0.00	41.27
$4^1\Pi$	Al ($3s^2 3d\ ^2D$) + F ($2s^2 2p^5\ ^2P$)	32435.453	36580.10	20.5	29.81

Notes. [a]Experimental data from the NIST Atomic Spectra Database (Kramida et al. 2020).
[b]Obtained from this work. The calculated energy of the $3^1\Sigma^+$ state reaches up to the largest internuclear distance of 8 Å due to the limit of the computing convergence. The $3^1\Sigma^+$ state does not seem to dissociate completely. The experimental energy of the dissociation limit of the $3^1\Sigma^+$ state is used in the calculation of the cross sections below.
[c]Estimated (see the text for details).
[d]Obtained from Martin & Zalubas (1979) and Yang et al. (2005).

Table 2. Spectroscopic constants of the $X^1\Sigma^+$, $A^1\Pi$, $2^1\Sigma^+$, and $3^1\Sigma^+$ states for AlF along with available experimental and theoretical values.

State	Source	R_e (Å)	T_e (cm^{-1})	ω_e (cm^{-1})	$\omega_e x_e$ (cm^{-1})	B_e (cm^{-1})	α_e (cm^{-1})	D_e (cm^{-1})
$X^1\Sigma^+$	This work	1.6639	0.00	801.64	5.791	0.5456	0.00514	57618.57
	Calc.[a]	1.6536	0.00	806.35	4.724	0.5530	0.00494	
	Calc.[b]	1.638	0.00	828.56	7.231	0.5632	0.00617	
	Calc.[c]	1.679	0.00	777				55410.27
	Expt.[d]	1.654[e]	0.00	802.4391	4.93269	0.55253	0.005	
$A^1\Pi$	This work	1.6551	44542.07	803.48	6.035	0.5521	0.00519	13682.94
	Calc.[b]	1.638	44924.57	807.89	8.644	0.5637	0.0076	
	Calc.[c]	1.679	44 387	764				
	Expt.[d]		43 949	804.15	6.047	0.5564	0.00534	
$2^1\Sigma^+$	This work	1.6241	54463.75	874.19	3.845	0.5734	0.00638	8829.44
	Calc.[b]	1.593	56352.80	938.65	8.988	0.5961	0.007	
	Expt.[d]		54 251	866.54	7.475	0.57967	0.0056	
$3^1\Sigma^+$	This work	1.6073	57985.24	923.81	5.335	0.58535	0.00394	12984.50
	Calc.[b]	1.57	58280.10	1152.94	22.248	0.61198	0.0052	
	Expt.[d]		57 688	938.20	5.087	0.58993	0.00459	

Notes. [a]Yousefi & Bernath (2018).
[b]Fitted by the vibrational levels calculated by Wells & Lane (2011).
[c]Langhoff et al. (1988).
[d]Fitted by the vibrational levels measured by Barrow et al. (1974).
[e]Zhang et al. (1995).

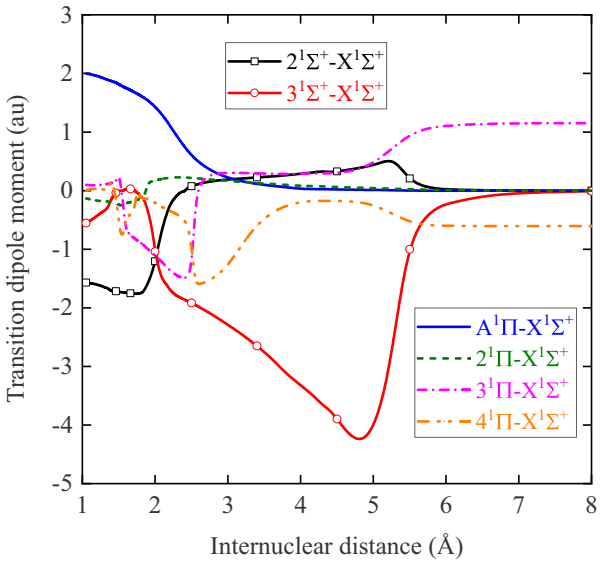

Figure 2. The TDMs from six low-lying excited $A^1\Pi$, $2^1\Sigma^+$, $3^1\Sigma^+$, $2^1\Pi$, $3^1\Pi$, and $4^1\Pi$ states to the ground $X^1\Sigma^+$ state. The symbols on the TDMs of the $2^1\Sigma^+$–$X^1\Sigma^+$ and $3^1\Sigma^+$–$X^1\Sigma^+$ transitions are data points displayed by skipping 10 points. All the data points are detailed in the text and provided in the supplemental material.

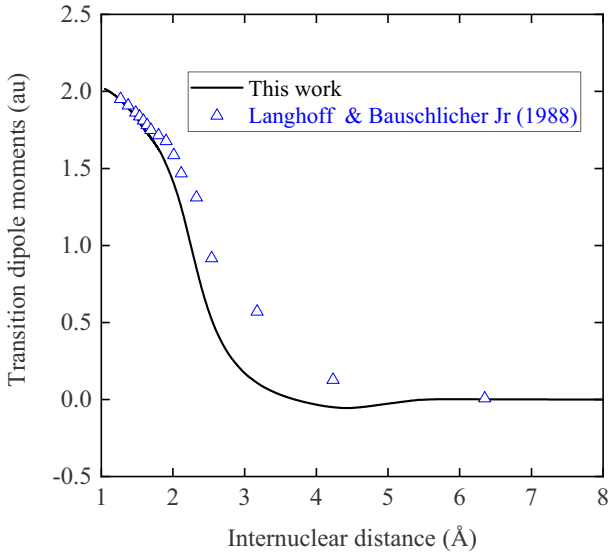

Figure 3. Comparison of TDMs for the $A^1\Pi$–$X^1\Sigma^+$ transition with those computed by Langhoff et al. (1988).

those of Langhoff et al. (1988). For the internuclear distances from 2 to 6 Å, our TDMs are slightly smaller than those of Langhoff et al. (1988), but the trends for these two sets of TDMs along the internuclear distance are the same.

Beyond the internuclear distances of 8 Å, the PECs and TDMs were extrapolated by fitting the long-range behaviours using the following formula:

$$V(R) = -\frac{C_5}{R^5} - \frac{C_6}{R^6} + V(R \to \infty), \tag{7}$$

where C_5 and C_6 are coefficients for each electronic state. For the short-range region down to a bond length of 0.8 Å, the PECs and TDMs were fitted by the following form:

$$V(R) = A \exp(-BR) + C, \tag{8}$$

in which A, B, and C are fitting parameters. The calculated *ab initio* points of PECs and TDMs were fitted by a cubic spline.

In this work, C_5 and C_6 are approximately estimated here. C_6 was estimated using the London formula

$$C_6 = \frac{3}{2}\frac{\Gamma_{Al}\Gamma_F}{\Gamma_{Al}+\Gamma_F}\alpha_{Al}\alpha_F, \tag{9}$$

where Γ_{Al} and Γ_F are ionization energies for a given Al atomic state and a given F atomic state, respectively. α_{Al} and α_F are dipole polarizabilities for Al and F, respectively, in a given atomic state. The ionization energies can be obtained from the NIST Atomic Spectra Database (Kramida et al. 2020). The dipole polarizability for Al, namely α_{Al}, is chosen to be 57.8 au for the ground state Al ($3s^2 3p\ ^2P$)

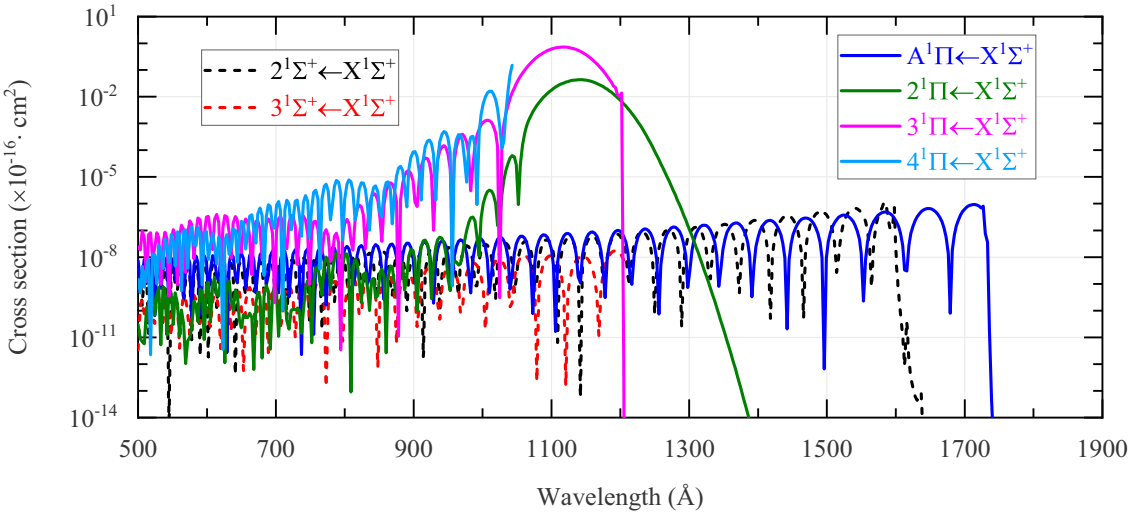

Figure 4. State-resolved cross sections of AlF for electronic transitions from the ground rovibrational level (υ'', J'') = (0, 0) to the $2^1\Sigma^+$, $3^1\Sigma^+$, $A^1\Pi$, $2^1\Pi$, $3^1\Pi$, and $4^1\Pi$ states.

(Schwerdtfeger & Nagle 2019). For the ground state F ($2s^22p^5\,{}^2P$), a dipole polarizability of 5.3 au is selected (Schwerdtfeger & Nagle 2019). No available dipole polarizabilities for excited states of Al are found, so we estimated the dipole polarizabilities of excited states Al ($3s^24s\,{}^2S$) and Al ($3s^23d\,{}^2D$) as the same value of the ground Al ($3s^23p\,{}^2P$) state here, just as done in previous publications (El-Qadi & Stancil 2013; Qin et al. 2021a). Note that the $3^1\Sigma^+$ state is associated with the ion-pair dissociation limit Al^+ ($3s^2\,{}^1S$) + F^- ($2s^22p^6\,{}^1S$). The dipole polarizability for Al^+ ($3s^2\,{}^1S$) and F^- ($2s^22p^6\,{}^1S$) is 24.3 au (Éhn & Cernušák 2020) and 14.5334 au (Wang et al. 2021), respectively. C_5 was estimated by fitting *ab initio* points while keeping the dissociation limits and C_6 fixed.

3.2 State-resolved and LTE cross sections

From the photodissociation theory and the computed PECs and TDMs, state-resolved cross sections were computed for transitions from 36 349 initial rovibrational levels ($\upsilon''\leq120$, $J''\leq360$) in the ground state to the $2^1\Sigma^+$, $3^1\Sigma^+$, $A^1\Pi$, $2^1\Pi$, $3^1\Pi$, and $4^1\Pi$ excited states with the photon wavelengths from 500 Å to the threshold. Fig. 4 shows a comparison of the state-resolved cross sections for each transition from the ground rovibrational level (υ'', $J''=0$, 0). As clearly seen, the $2^1\Pi$–$X\ {}^1\Sigma^+$, $3^1\Pi$–$X\ {}^1\Sigma^+$, and $4^1\Pi$–$X\ {}^1\Sigma^+$ transitions contribute significantly to the cross sections for lower wavelengths, especially between the Lyman and Lyman α ones, where the emission spectrum is known to be of high intensity in some astrophysical situations, including fast shocks (Neufeld & Dalgarno 1989; Agúndez et al. 2012) and young stars (Valenti, Johns-Krull & Linsky 2000; Yang et al. 2012). Other transitions make relatively small contributions. The state-resolved cross sections are relatively large for the $3\ {}^1\Pi\leftarrow X\ {}^1\Sigma^+$ transition; the variation of the cross sections with vibrational and rotational quantum numbers is shown in Fig. 5. Cross sections are plotted in Fig. 5(a) from several vibrational levels with the rotational quantum number $J''=0$ and in Fig. 5(b) from several rotational levels with the vibrational quantum number $\upsilon''=0$.

The LTE cross sections are then computed by assuming a Boltzmann population distribution for the rovibrational levels in the ground state for each transition from 50 to 20 000 K in 50 K intervals. A comparison of the LTE cross sections for each transition at 2000 K is shown in Fig. 6. Below about 800 Å, the $3^1\Sigma^+\leftarrow X^1\Sigma^+$ and $3^1\Pi\leftarrow X\ {}^1\Sigma^+$ transitions dominate most. At wavelengths from around 800 to 1700 Å, the $2^1\Pi\leftarrow X\ {}^1\Sigma^+$ and $3^1\Pi\leftarrow X\ {}^1\Sigma^+$ transitions are dominated. At wavelengths from about 1700 to 2100 Å, the $2^1\Sigma^+\leftarrow X^1\Sigma^+$ transition contributes most. Above 2100 Å, the $A^1\Pi\leftarrow X\ {}^1\Sigma^+$ transition makes a significant contribution. To exhibit temperature-dependent behaviour of the LTE cross sections, a sample of the cross sections for the $3\ {}^1\Pi\leftarrow X\ {}^1\Sigma^+$ transition at several temperatures from 500 to 20 000 K is shown in Fig. 7.

3.3 Photodissociation rates

The presence of AlF was confirmed in the circumstellar envelope of the carbon star IRC + 10216 (Agúndez et al. 2012). Due to the lack of the photodissociation rate for AlF, Agúndez et al. (2012) utilized the visual extinction to approximately estimate the AlF photodissociation rate, which may introduce uncertainties in its derived abundance. Here, the photodissociation rates for AlF are computed. We concentrate on the ISRF and blackbody radiation field since both are widely used in astrochemical community. Photodissociation rates in ISRF are calculated by using the state-resolved cross sections (υ'', J'') = (0, 0) and LTE cross sections below 300 K and presented in Table 3. The results show that the largest contribution to the total photodissociation rate is from the $3^1\Pi\leftarrow X\ {}^1\Sigma^+$ transition, accounting for about 92 per cent. This situation is similar to the investigation of ISRF photodissociation rate for AlCl, in which its $3^1\Pi\leftarrow X\ {}^1\Sigma^+$ transition contributes significantly (Qin, Bai & Liu 2021b). Such similarity may be from the fact that AlCl and AlF are members of the aluminium monohalide family. In the blackbody radiation field, the temperature-dependent photodissociation rates of AlF in LTE are computed for the studied six electronic transitions and displayed in Fig. 8. As shown in Fig. 8, the $A^1\Pi\leftarrow X\ {}^1\Sigma^+$ transition contributes most for the considered temperature range from 500 to 20 000 K.

Here, we considered the highest electronic state of $4^1\Pi$, which dissociates into the Al ($3s^24s\,{}^2D$) + F ($2s^22p^5\,{}^2P$) asymptote. Above this asymptote, there exist other higher singlet $^1\Sigma^+$ and $^1\Pi$ states, which may also contribute to the direct photodissociation cross sections below about 3085 Å. Especially, the thresholds of the cross sections for transitions from the ground rovibrational levels (υ'',

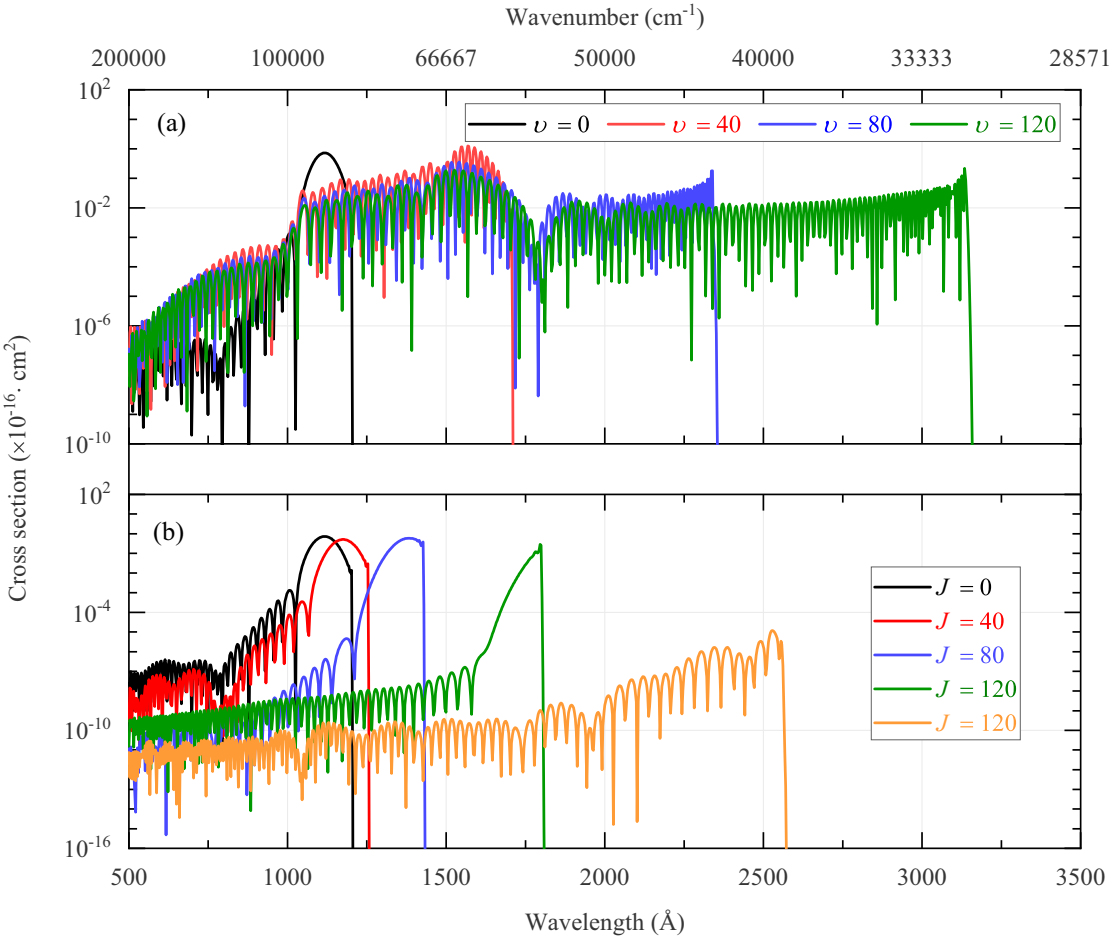

Figure 5. State-resolved cross sections of AlF for the $3^1\Pi \leftarrow X^1\Sigma^+$ transition from (a) several vibrational levels with the rotational quantum number $J'' = 0$ and (b) several rotational levels with the vibrational quantum number $\upsilon'' = 0$.

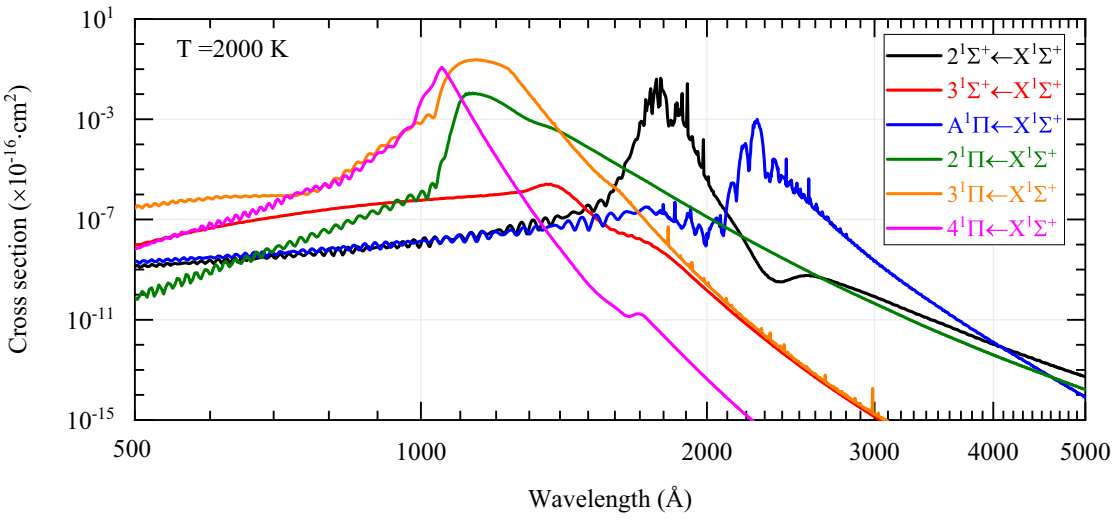

Figure 6. The LTE cross sections at 2000 K for transitions from the $X^1\Sigma^+$ state to the six excited singlet states.

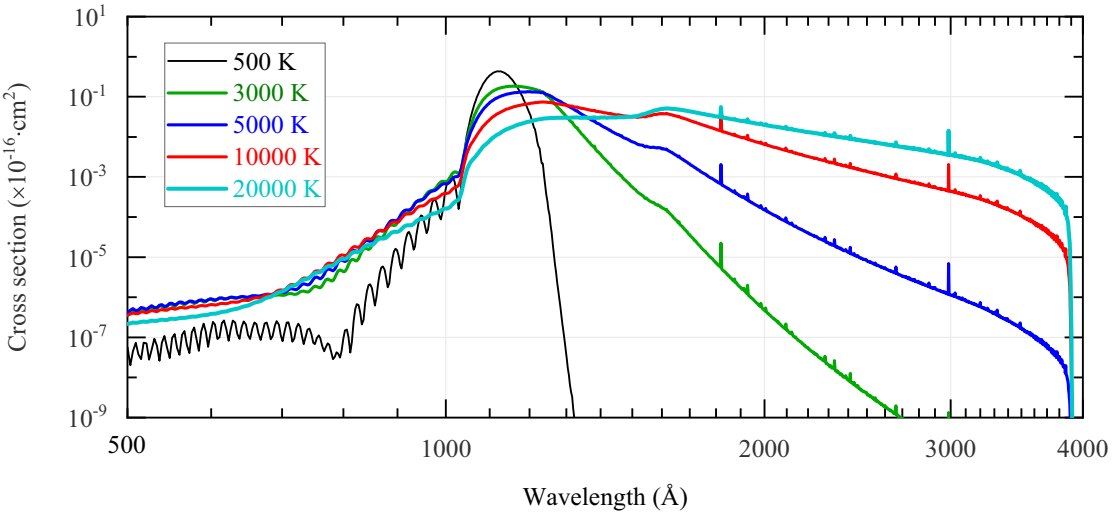

Figure 7. The LTE cross sections for the $3^1\Pi \leftarrow X^1\Pi$ transition at several kinetic temperatures.

Table 3. Photodissociation rates (s^{-1}) of AlF under the standard ISRF.

Transition	State-resolved cross section	LTE cross section				
	$(v'', J'') = (0, 0)$	10 K	50 K	100 K	200 K	300 K
$2^1\Sigma^+ \leftarrow X^1\Sigma^+$	1.48×10^{-15}	1.57×10^{-15}	1.85×10^{-15}	1.70×10^{-15}	1.50×10^{-15}	1.44×10^{-15}
$3^1\Sigma^+ \leftarrow X^1\Sigma^+$	2.29×10^{-17}	2.28×10^{-17}	2.27×10^{-17}	2.26×10^{-17}	2.27×10^{-17}	2.56×10^{-17}
$A^1\Pi \leftarrow X^1\Sigma^+$	2.12×10^{-15}	1.54×10^{-15}	1.68×10^{-15}	1.51×10^{-15}	1.31×10^{-15}	1.23×10^{-15}
$2^1\Pi \leftarrow X^1\Sigma^+$	5.92×10^{-11}	4.09×10^{-11}	3.98×10^{-11}	3.96×10^{-11}	3.95×10^{-11}	3.94×10^{-11}
$3^1\Pi \leftarrow X^1\Sigma^+$	8.70×10^{-10}	6.01×10^{-10}	5.86×10^{-10}	5.85×10^{-10}	5.87×10^{-10}	5.90×10^{-10}
$4^1\Pi \leftarrow X^1\Sigma^+$	1.24×10^{-11}	8.44×10^{-12}	7.69×10^{-12}	7.22×10^{-12}	7.09×10^{-12}	8.34×10^{-12}
All $^1\Pi \leftarrow X^1\Sigma^+$	9.42×10^{-10}	6.50×10^{-10}	6.33×10^{-10}	6.32×10^{-10}	6.34×10^{-10}	6.38×10^{-10}
Total	9.42×10^{-10}	6.50×10^{-10}	6.33×10^{-10}	6.32×10^{-10}	6.34×10^{-10}	6.38×10^{-10}

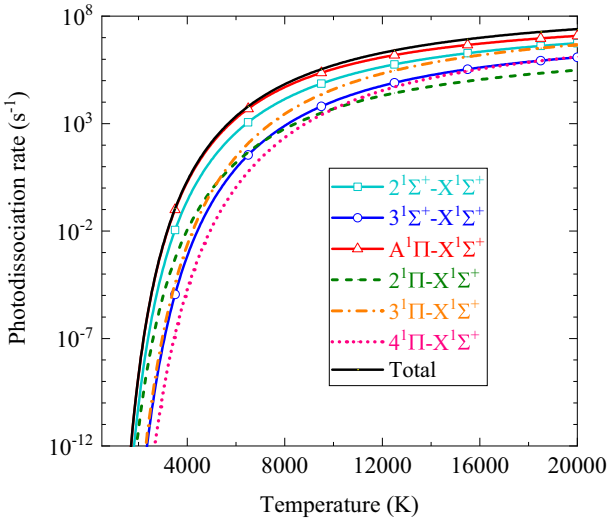

Figure 8. Photodissociation rates for each electronic transition of AlF exposed to a blackbody radiation field at temperatures from 500 to 20 000 K.

$J'' = 0$) to the higher singlet $^1\Sigma^+$ and $^1\Pi$ states may contribute to the interstellar radiation at wavelengths from about 946 to 1062 Å. Moreover, predissociation may be dominated at wavelengths longer than 1400 Å, where the direct photodissociation cross sections are small. Hence, the photodissociation rates presented here are lower limits.

4 CONCLUSION

Photodissociation cross sections and rates of AlF have been studied using high-level *ab initio* PECs and TDMs. These data are of great interest to astrochemical community as AlF has been observed in the circumstellar envelope of the carbon star IRC + 10216, but a lack of photodissociation data is hampering the accurate prediction of its abundance. PECs and TDMs have been produced at the icMRCI + Q/aug-cc-pCV5Z level of theory to perform comprehensive calculations of photodissociation cross sections and rates of AlF through $2^1\Sigma^+ \leftarrow X^1\Sigma^+$, $3^1\Sigma^+ \leftarrow X^1\Sigma^+$, $A^1\Pi \leftarrow X^1\Sigma^+$, $2^1\Pi \leftarrow X^1\Sigma^+$, $3^1\Pi \leftarrow X^1\Sigma^+$, and $4^1\Pi \leftarrow X^1\Sigma^+$ transitions. The state-resolved cross sections and temperature-dependent LTE cross sections have been computed for the rovibrational transitions from a total of 36 349 rovibrational levels in the ground state ($v'' \leq 120$, $J'' \leq 360$) over a large range of wavelengths. Photodissociation rates of AlF dissociated by the ISRF and blackbody radiation field have been then determined by using the cross sections. The obtained photodissociation cross sections and rates of AlF can be used to securely derive its abundance in the circumstellar envelope of the carbon star IRC + 10216.

ACKNOWLEDGEMENTS

The supports from National Natural Science Foundation of China (52106098, 51421063) are acknowledged. ZQ also acknowledges the support from Natural Science Foundation of Shandong Province (ZR2021QE021), China Postdoctoral Science Founda-

tion (2021M701977), Postdoctoral Innovation Project of Shandong Province, and Postdoctoral Applied Research Project of Qingdao City. The scientific calculations in this paper have been done on the HPC Cloud Platform of Shandong University.

DATA AVAILABILITY

Full data are available. The cross sections and rate coefficients can be obtained online via https://dr-zhi-qin.github.io/personal/Database.html. The supplemental materials include the PECs and TDMs for AlF (corresponding to Figs 1 and 2), as well as its LTE photodissociation rates in the blackbody radiation field (corresponding to Fig. 8).

CONFLICT OF INTEREST

There are no conflicts to declare.

REFERENCES

Agúndez M., Fonfría J. P., Cernicharo J., Kahane C., Daniel F., Guélin M., 2012, A&A, 543, A48
Andreazza C. M., de Almeida A. A., 2014, MNRAS, 437, 2932
Babb J. F., 2015, ApJS, 216, 21
Bagare S. P., Kumar K. B., Rajamanickam N., 2006, Sol. Phys., 234, 1
Bai T., Qin Z., Liu L., 2021, MNRAS, 505, 2177
Barrow R. F., Kopp I., Malmberg C., 1974, Phys. Scr., 10, 86
Cernicharo J., Guélin M., 1987, A&A, 183, L10
Draine B. T., 1978, ApJS, 36, 595
Éhn L., Cernušák I., 2020, Int. J. Quantum Chem., 121, e26467
El-Qadi W. H., Stancil P. C., 2013, ApJ, 779, 97
Gao H., 2020, Mol. Phys., 119, e1861354
Gay C. D., Abel N. P., Porter R. L., Stancil P. C., Ferland G. J., Shaw G., Van Hoof P. A. M., Williams R. J. R., 2012, ApJ, 746, 78
Gotoum N., Hammami K., Owono L. C. O., Jaidane N.-E., 2012, Ap&SS, 337, 553
Gotoum N., Nkem C., Hammami K., Charfadine M. A., Owono L. C. O., Jaidane N.-E., 2011, Ap&SS, 332, 209
Hansson A., Watson J. K. G., 2005, J. Mol. Spectrosc., 233, 169
Heays A. N., Bosman A. D., van Dishoeck E. F., 2017, A&A, 602, A105
Highberger J. L., Savage C., Bieging J. H., Ziurys L. M., 2001, ApJ, 562, 790

Kamiński T. et al., 2018, Nat. Astron., 2, 778
Kirby K. P., Van Dishoeck E. F., 1989, Adv. At. Mol. Phys., 25, 437
Knowles P. J., Werner H.-J., 1985, Chem. Phys. Lett., 115, 259
Kramida A., Ralchenko Y., Reader J., NIST ASD Team, 2020, NIST Atomic Spectra Database (version 5.8). Available at: https://physics.nist.gov/asd
Langhoff S. R., Bauschlicher C. W., Jr, Taylor P. R., 1988, J. Chem. Phys., 88, 5715
Martin W. C., Zalubas R., 1979, J. Phys. Chem. Ref. Data, 8, 817
Mauron N., Huggins P. J., 2010, A&A, 513, A31
McMillan E. C., Shen G., McCann J. F., McLaughlin B. M., Stancil P. C., 2016, J. Phys. B: At. Mol. Opt. Phys., 49, 084001
Miyake S., Gay C. D., Stancil P. C., 2011, ApJ, 735, 21
Neufeld D. A., Dalgarno A., 1989, ApJ, 344, 251
Pattillo R. J., Cieszewski R., Stancil P. C., Forrey R. C., Babb J. F., McCann J. F., McLaughlin B. M., 2018, ApJ, 858, 10
Qin Z., Bai T., Liu L., 2021a, ApJ, 917, 87
Qin Z., Bai T., Liu L., 2021b, MNRAS, 508, 2848
Reiher M., Wolf A., 2004a, J. Chem. Phys., 121, 2037
Reiher M., Wolf A., 2004b, J. Chem. Phys., 121, 10945
Schlemmer S., Mutschke H., Giesen T., Jäger C., 2014, Laboratory Astrochemistry. Wiley-VCH, Weinheim
Schwerdtfeger P., Nagle J. K., 2019, Mol. Phys., 117, 1200
Stancil P., Kirby K., Sannigrahi A. B., Buenker R. J., Hirsch G., Gu J.-P., 1997, ApJ, 486, 574
Turner B. E., 1991, ApJ, 376, 573
Valenti J. A., Johns-Krull C. M., Linsky J. L., 2000, ApJS, 129, 399
Valiev R. R., Berezhnoy A. A., Gritsenko I. S., Merzlikin B. S., Cherepanov V. N., Kurten T., Wöhler C., 2020, A&A, 633, A39
van Dishoeck E. F., Black J. H., 1982, ApJ, 258, 533
van Dishoeck E. F., Black J. H., 1988, ApJ, 334, 771
Wang K., Wang X., Fan Z., Zhao H.-Y., Miao L., Yin G.-J., Moro R., Ma L., 2021, Eur. Phys. J. D, 75, 46
Watson J. K., 2008, J. Mol. Spectrosc., 252, 5
Weck P. H., Stancil P. C., Kirby K., 2003, ApJ, 582, 1263
Wells N., Lane I. C., 2011, Phys. Chem. Chem. Phys., 13, 19018
Werner H. J. et al., 2015, MOLPRO 2015, a package of ab initio programs, see http://www.molpro.net
Werner H. J. et al., 2020, J. Chem. Phys., 152, 144107
Werner H. J., Knowles P. J., 1985, J. Chem. Phys., 82, 5053
Yang H. et al., 2012, ApJ, 744, 121
Yang J., Hao Y., Li J., Zhou C., Mo Y., 2005, J. Chem. Phys., 122, 134308
Yousefi M., Bernath P. F., 2018, ApJS, 237, 8
Zhang K. Q., Guo B., Braun V., Dulick M., Bernath P. F., 1995, J. Mol. Spectrosc., 170, 82
Ziurys L. M., Apponi A. J., Phillips T. G., 1994, ApJ, 433, 729
Ziurys L. M., Savage C., Highberger J. L., Apponi A. J., Guélin M., Cernicharo J., 2001, ApJ, 564, L45

SUPPORTING INFORMATION

Supplementary data are available at *MNRAS* online.

Potential_energy.txt
Transition_dipole_moment.txt
Photodissociation_rate.txt

Please note: Oxford University Press is not responsible for the content or functionality of any supporting materials supplied by the authors. Any queries (other than missing material) should be directed to the corresponding author for the paper.

This paper has been typeset from a TEX/LATEX file prepared by the author.